Optical properties of a $Cr^{3+}$-doped fluorophosphate glass investigated by steady state and time-resolved laser spectroscopy



1992 J. Phys.: Condens. Matter 4 10323

(http://iopscience.iop.org/0953-8984/4/50/019)

J. Phys.: Condens. Matter 4 (1992) 10323–10334. Printed in the UK

# Optical properties of a $Cr^{3+}$-doped fluorophosphate glass investigated by steady state and time-resolved laser spectroscopy

Rolindes Balda, Joaquín Fernández and Mª Asunción Illarramendi

Departamento de Fisica Aplicada I, Escuela Técnica Superior de Ingenieros Industriales y de Telecomunicación, Universidad del País Vasco, Alameda de Urquijo s/n 48013 Bilbao, Spain

Received 11 August 1992, in final form 22 September 1992

**Abstract.** The optical properties of trivalent-chromium-doped fluorophosphate glass (21.74 $Al(PO_3)_3$–57.8 $BaF_2$–16.96 $AlF_3$ (wt.%)) have been investigated in the 4.2–300 K temperature range using steady state and time-resolved laser spectroscopy. The luminescence of $Cr^{3+}$ shows a strong thermal quenching which can be analysed in terms of the quantum mechanical single-configurational coordinate model. In order to establish a correlation between the glass matrix composition and the spectral and temperature behaviour of the $Cr^{3+}$ photoluminescence, detailed time-resolved measurements have been performed. When compared with fluoride glasses, the results attained for the emission wavelength dependence of the lifetimes and excitation spectra show an enhancement of the site-dependent effects.

## 1. Introduction

The optical properties of $Cr^{3+}$-doped glasses have attracted much attention over the past few years [1–12]. The absorption and emission of $Cr^{3+}$ arises from the parity-forbidden electronic transitions in the 3d electronic shell. Crystal-field-split states of $Cr^{3+}$ octahedral symmetry are illustrated in the diagrams of Sugano *et al* [13]. The relative positions of the excited $^4T_2$ and $^2E$ states depend on the crystal-field strength. For $Dq/B < 2.3$ (low-field cases), $^4T_2$ is the lowest excited state and the emission arises from the $^4T_2$-to-$^4A_2$ spin-allowed transition. These $^4T_2 \leftrightarrow {}^4A_2$ broad absorption and emission bands are of interest for applications in lasers [14] and solar concentrators [15]. This transition is also responsible for the efficient sensitization of $Nd^{3+}$ if energy transfer from $Cr^{3+}$ to $Nd^{3+}$ is more probable than radiative or non-radiative relaxation of the $^4T_2$ state. In addition to these potential applications, $Cr^{3+}$ ions are also useful as a spectroscopic probe for obtaining information about the amorphous local environment [16]. In most glasses, $Cr^{3+}$ ions occupy sites which have nearly octahedral symmetry because of the strong ligand-field stabilization energy of $Cr^{3+}$ in a sixfold coordination.

Recently the present authors and co-workers [8–11] have discussed the optical properties of $Cr^{3+}$ ions in nearly octahedral sites, in several heavy-metal fluoride glasses (HMFGs) and transition-metal fluoride glasses (TMFGs). These glasses are low-field glasses for which the emission is characterized by the $^4T_2 \rightarrow {}^4A_2$ transition. The

0953-8984/92/5010323+12$07.50  

width of the optical spectra showed that $Cr^{3+}$ ions occupy a range of slightly distorted octahedral sites. The site effects and the correlation between glass matrix composition and emission spectral properties were studied using detailed steady state and time-resolved laser spectroscopy. The spectroscopic data indicated the existence of two main site distributions for $Cr^{3+}$ ions in these fluoride glasses. In these studies the thermal quenching of the luminescence was also discussed in terms of the quantum mechanical single-configurational-coordinate (QMSCC) model [17], and the parameters obtained from this model correlated well with the influence of the host material on the quantum efficiency (QE) of $Cr^{3+}$.

In the present work, we have extended this analysis of the optical properties of $Cr^{3+}$ to a mixed-fluorophosphate glass, paying attention to the influence of the glass composition on the spectral and temperature behaviours of the $Cr^{3+}$ photoluminescence. In order to establish further correlation between the results obtained for fluorophosphate and fluoride glasses, some comparative results are given which provide evidence of the enhancement of the site-dependent effects in the fluorophosphate glass.

## 2. Experimental techniques

Fluorophosphate glass samples were obtained with the composition 21.74 $Al(PO_3)_3$–57.8 $BaF_2$–16.96 $AlF_3$ and doped with 0.5 wt% $Cr_2O_3$. The glass was prepared by melting the precursor mixture in platinum crucibles in an electric furnace heated to 1200 ° in a controlled atmosphere. Then the melt was poured into a brass mould and annealed at 500 °C. Finally, the samples were cut and polished for optical measurements.

The sample temperature was varied between 4.2 and 300 K with a continuous-flow cryostat. Conventional absorption spectra were performed with a Cary 17 spectrophotometer. The emission measurements were made using the 633 nm emission line of a 15 mW He–Ne laser and the 514 nm of an argon laser as exciting light, which was chopped at 200 Hz. The fluorescence was analysed with a 0.22 m Spex monochromator, and the signal was detected with a Hamamatsu R7102 extended IR photomultiplier and finally amplified by a standard lock-in technique. The system response was calibrated with a standard tungsten–halogen lamp which was also calibrated against a National Bureau of Standards lamp, in order to correct the emission spectra.

Lifetime measurements were performed with a tunable dye laser (1 ns pulse width), pumped by a pulsed nitrogen laser. In order to describe the evolution of fluorescence, time-resolved spectroscopy has been used. The emission measurements were obtained by exciting the sample with a tunable dye laser and detecting the emission with a Hamamatsu R7102 photomultiplier. The lifetimes and time-resolved emission spectra were processed by a EGG-PAR boxcar integrator.

## 3. Experimental results

### *3.1. Absorption and emission spectra*

The location and features of the absorption bands of $Cr^{3+}$-doped glasses can be accounted for by using the ligand-field theory if one assumes that, on the average,

the chromium ions occupy sites which have nearly octahedral symmetry [1, 2, 18]. Therefore the absorption and emission spectra are usually interpreted using the diagram of Sugano *et al* [13] for $d^3$ systems with octahedral coordination, at least as far as the energy levels are concerned [2].

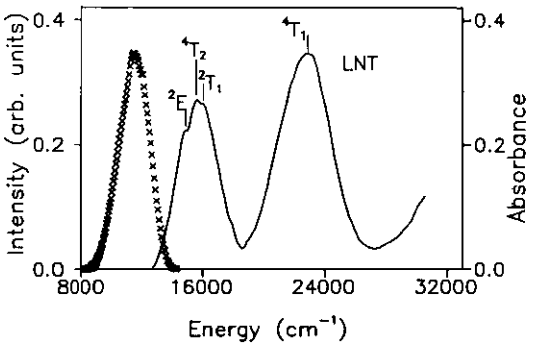


**Figure 1.** Absorption (——) and emission (×) spectra at LNT for $Cr^{3+}$-doped fluorophosphate glass. The emission spectra were corrected for instrumental response and were obtained under excitation with the 633 nm line of a He–Ne laser.

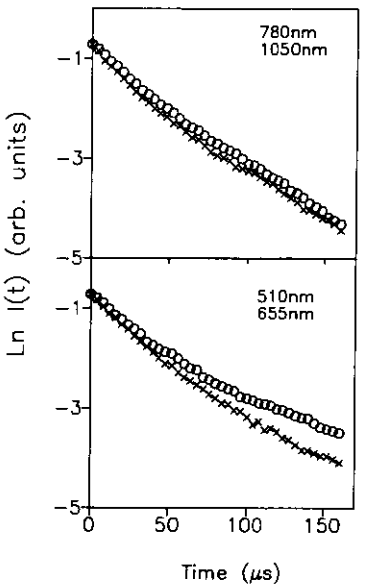


**Figure 2.** (*a*) Logarithmic plot of the $^4T_2 \rightarrow {}^4A_2$ decays monitored at 780 nm (○) and 1050 nm (×), for an excitation wavelength of 655 nm. (*b*) Logarithmic plot of the decays monitored at 890 nm for different excitation wavelengths: (○), 510 nm; (×), 655 nm. The measurements were performed at 77 K.

The absorption and emission spectra have been measured as a function of temperature in the 4.2 K–300 K temperature range. Figure 1 shows the emission and absorption spectra of $Cr^{3+}$-doped fluorophosphate glass obtained at liquid-nitrogen temperature (LNT). The absorption spectrum shows two broad bands due to the transitions from the $^4A_2$ ground state to the $^4T_2$ and $^4T_1$ excited states. The low-energy band shows a fine structure at 14818 $cm^{-1}$ and 15795 $cm^{-1}$ due to the spin-forbidden transitions $^4A_2 \rightarrow {}^2E$ and $^4A_2 \rightarrow {}^2T_1$, respectively. The assignment of this structure has been made following the Fano antiresonance interpretation [19–21].

The experimental energies of the absorption bands may be used to determine the strength $Dq$ of the octahedral crystal field and the Racah parameters. Because of the inherent disorder due to the glass structure these values represent an average over the distribution of sites occupied by the $Cr^{3+}$ ions in the glass. Table 1 compares the LNT spectroscopic data for $Cr^{3+}$ absorption in the fluorophosphate glass and in two HMFG. As can be seen, the fluorophosphate glass presents a higher value for $Dq/B$, and the absorption bands shifted to higher energies. The $Dq/B$-values show that these glasses provide low-field sites for $Cr^{3+}$ ions in which the energy in the $^4T_2$ level is lower than in the $^2E$ level for all sites. In consequence, the emission is characterized

**Table 1.** LNT absorption spectroscopic data for $Cr^{3+}$-doped fluorophosphate and fluoride glasses. The data for ZBLAN and BIGAZYT were taken from [8] and [9], respectively.

| | Value for the following glasses | | |
|---|---|---|---|
| Parameter | ZBLAN | BIGAZYT | Fluorophosphate |
| $^4A_2 \rightarrow {}^4T_2$ ($cm^{-1}$) | 15138 | 15487 | 15742 |
| $^4A_2 \rightarrow {}^4T_1$ ($cm^{-1}$) | 22123 | 22714 | 22727 |
| $^4A_2 \rightarrow {}^2E$ ($cm^{-1}$) | 15208 | 15267 | 14818 |
| $^4A_2 \rightarrow {}^2T_1$ ($cm^{-1}$) | 15966 | 16129 | 15795 |
| $Dq/B$ | 1.96 | 2.01 | 2.16 |

by a broad Stokes-shifted band centred in the near infrared, which corresponds to the $^4T_2 \rightarrow {}^4A_2$ emission. The emission spectrum in figure 1, corresponding to the fluorophosphate glass, was obtained under excitation in the $^4A_2 \rightarrow {}^4T_2$ absorption band using the 633 nm line of a He–Ne laser. Additional measurements under excitation in the $^4A_2 \rightarrow {}^4T_1$ absorption band will also be given in section 4.2. Table 2 presents the LNT emission spectroscopic data for this glass including data for two HMFGS for comparison. The $^4T_2$ emission peak position was used to determine a value of $Dq/B$ for the relaxed excited state from the formula

$$(Dq/B)_{RES} = E\left({}^4T_2 \rightarrow {}^4A_2\right)/10B. \tag{1}$$

As can be seen, the high crystal field for the fluorophosphate glass results in a blue shift of the emission band when compared with the corresponding band for fluorides. In the same way as for fluoride glasses a large Stokes shift (about 4200 $cm^{-1}$) is observed, indicating that a considerable change occurs in the ionic arrangement around $Cr^{3+}$ in the excited state [4, 22]. The integrated emission intensity is strongly dependent on temperature, being quenched at 295 K to 5% of its value at 4.2 K.

**Table 2.** LNT emission spectroscopic data of $Cr^{3+}$-doped fluorophosphate and fluoride glasses. The data for ZBLAN and BIGAZYT were taken from [8] and [9], respectively. $\sigma$ is the half-width of $^4T_2 \rightarrow {}^4A_2$ emission, $(Dq/B)_{RES}$ is the crystal field for the relaxed excited state, $\Delta E_S$ is the Stokes shift and $\tau_{exp}$ is the average lifetime monitored at the emission peak.

| | Value for the following glasses | | |
|---|---|---|---|
| Parameter | ZBLAN | BIGAZYT | Fluorophosphate |
| $^4T_2 \rightarrow {}^4A_2$ ($cm^{-1}$) | 11178 | 11498 | 11519 |
| $\sigma$ ($cm^{-1}$) | 932 | 1086 | 997 |
| $(Dq/B)_{RES}$ | 1.45 | 1.48 | 1.58 |
| $\Delta E_S$ ($cm^{-1}$) | 3960 | 4027 | 4223 |
| $\tau_{exp}$ ($\mu s$) | 99 | 72 | 40 |

### *3.2. Analysis of Fano antiresonances in absorption spectra*

In figure 1 the low-energy $^4A_2 \rightarrow {}^4T_2$ absorption band of $Cr^{3+}$ obtained at LNT was shown. This band has a fine structure due to the intraconfigurational transitions $^4A_2 \rightarrow {}^2E$, $^2T_1$ which are interpreted as Fano antiresonances.

**Table 3.** Parameters of $^2E$ antiresonances at LNT. $\gamma$ indicates the spectral width of the autoionized state, and $E_r$ is the antiresonance energy. The data for ZBLAN and BIGAZYT glasses were taken from [21].

| | Values for the following glasses | | |
|---|---|---|---|
| Parameter | ZBLAN | BIGAZYT | Fluorophosphate |
| $\rho^2$ | 0.17 | 0.22 | 0.11 |
| $q$ | 0.11 | −0.105 | −0.27 |
| $\gamma$ ($cm^{-1}$) | 170 | 214 | 175 |
| $E_r$ ($cm^{-1}$) | 15238 | 15245 | 14818 |

Following a similar analysis to that used by the present authors [21] for HMFGS and TMFGS, the parameters of $^2E$ and $^2T_1$ antiresonances were obtained.

Table 3 shows the LNT parameters of the $^2E$ antiresonance in this glass including data on two HMFGS [21] for comparison. The value obtained for $\rho^2$ (the fraction of band states involved in the interference processes) is smaller than those obtained in HMFGS, showing that this fluorophosphate glass is a more ordered system. The small values obtained for $q$ (the numerical index which characterizes the line profile) in all cases indicate that the antiresonances are produced by a sharp forbidden transition overlapping a broad allowed transition.

### *3.3. Emission lifetime results*

The time behaviour of the $Cr^{3+}$ fluorescence decay in fluorophosphate glass has been studied as a function of temperature, emission and excitation wavelength.

The observed decays measured along the broad emission band, under pulsed-laser excitation, at the $^4A_2 \rightarrow {}^4T_2$ and $^4A_2 \rightarrow {}^4T_1$ absorption bands, are multi-exponential throughout the whole temperature range. Figure 2(*a*) shows, as an example, the logarithmic plot of the intensity decay (excited at 655 nm) at LNT for emission wavelengths on the blue and red sides of the emission band. From the figure, it can be seen that the time dependence of the decays varies slightly across the broad emission band, shifting towards shorter decay times as the wavelength increases. In addition to the spectral dependence of the decays, a dependence on the excitation wavelength is also observed. These data are plotted in figure 2(*b*) which shows the time decays of the luminescence monitored at 890 nm at two different excitation wavelengths. The excitations correspond to the energies of the peak position of the $^4A_2 \rightarrow {}^4T_2$ (655 nm), and the low-energy side of the $^4A_2 \rightarrow {}^4T_1$ (510 nm) absorption bands, respectively. The best fit of the decay curves corresponds to a double-exponential function. The short-lived and long-lived components of the experimental decays obtained by a least-squares fit are around 22 $\mu$s and 76 $\mu$s, respectively, at LNT for an emission wavelength of 890 nm under excitation at 655 nm.

For practical purposes we shall use the 'average lifetime' defined by the equation $\bar{\tau} = (\int tI(t)\,dt)/(\int I(t)\,dt)$ in the analysis which follows.

The spectral dependence of the decays along the broad emission band obtained at two different excitation wavelengths (510 and 655 nm) are plotted in figure 3. As can be seen for excitation in the peak position of the $^4A_2 \rightarrow {}^4T_2$ absorption band, the lifetimes remain nearly constant at the shortest wavelengths and then decrease as the wavelength increases. By contrast, for excitation on the low-energy side of the $^4A_2 \rightarrow {}^4T_1$ absorption band, the lifetimes decrease as the wavelength increases

throughout the emission band. This behaviour can be qualitatively understood by taking into account the fact the 510 nm excitation mainly results in absorption processes at weaker field sites whereas, under 655 nm excitation, stronger field sites are mainly involved.

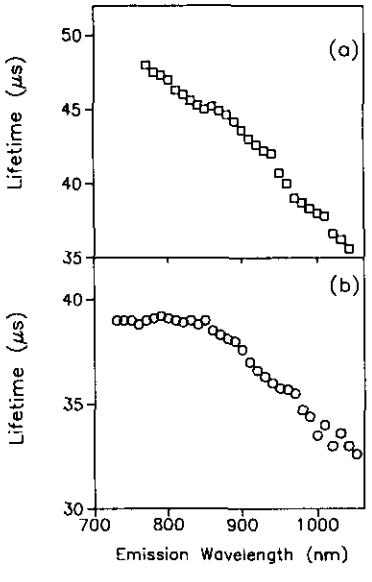


**Figure 3.** LNT lifetimes at different emission wavelengths along the $^4T_2 \rightarrow {}^4A_2$ emission band for two excitation wavelengths: (*a*) 510 nm; (*b*) 655 nm. The data correspond to the average lifetime.

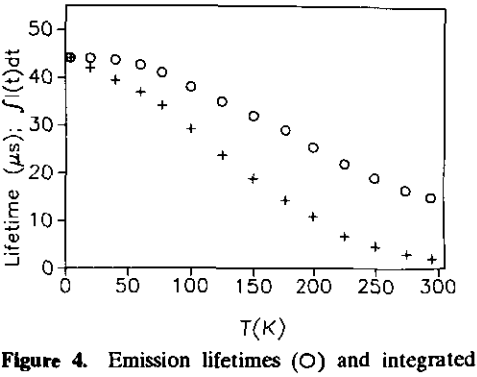


**Figure 4.** Emission lifetimes (O) and integrated emission intensities (+) as functions of temperature for $Cr^{3+}$-doped fluorophosphate glass, obtained by excitation at 655 nm and collecting the fluorescence at the peak position of the emission band.

Lifetime data, obtained under excitation at 655 nm and monitored at the peak position of the emission bands, and integrated emission intensities $\int I(t)\ dt$, as functions of temperature are shown in figure 4. It is apparent from this figure that the emission lifetimes and the integrated intensities display similar qualitative behaviours with temperature.

### *3.4. Time-resolved spectra*

The variation in fluorescence lifetime with emission wavelength, and the multi-exponential character of the decays suggested the existence of some kind of site distribution for the $Cr^{3+}$ ions. These site effects are also evidenced by the time-resolved excitation and emission spectra.

The excitation spectra were obtained at 4.2 and 77 k by exciting the sample with a tunable dye laser and collecting the luminescence at different wavelengths along the $^4T_2 \rightarrow {}^4A_2$ emission band, and at different time delays. Figure 5(*a*) shows the LNT excitation spectra for luminescence monitored at 780 nm (on the high-energy wing of the emission band), and at 1030 nm (on the low-energy wing) at a time delay of 1 μs (gate width, 20 ns). As is easily seen, the high-energy spectrum is blue shifted corresponding to the emission from high-energy sites. Figure 5(*b*) presents the LNT

excitation spectra performed at two time delays (1 and 150 $\mu$s (gate width, 1 $\mu$s)) for luminescence monitored at 880 nm. The decrease in the excitation band width obtained at 150 $\mu$s corresponds to the emission losses from the low field sites. Since only the qualitative comparison between spectra was of interest, no corrections were made for the dye laser.

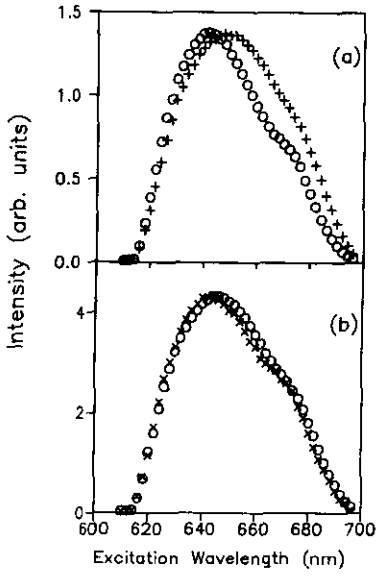


**Figure 5.** (*a*) LNT excitation spectra of the $^4T_2 \rightarrow {}^4A_2$ transition at a time delay of 1 $\mu$s for luminescence monitored at 780 nm (○) and 1030 nm (+). (*b*) LNT excitation spectra for luminescence monitored at 890 nm at two time delays: (○), 1 $\mu$s; (×) 150 $\mu$s.

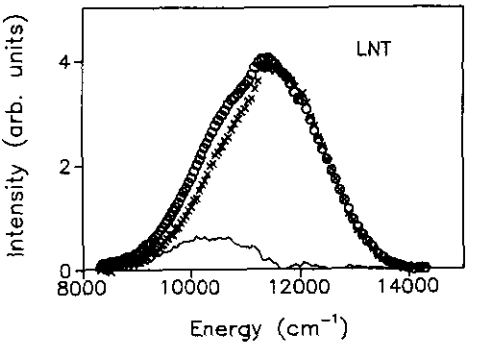


**Figure 6.** Comparison between the scaled time-resolved emission spectrum of $^4T_2 \rightarrow {}^4A_2$ transition at a time delay of 150 $\mu$s (×), and steady state emission spectrum (○): difference between the two spectra (——). The steady state spectra was obtained by excitation at 633 nm, and the time-resolved spectra by excitation at 655 nm. The measurements were performed at 77 K.

Time-resolved emission spectra were obtained at 77 K after exciting the samples with a tunable laser at the peak position of the $^4A_2 \rightarrow {}^4T_2$ absorption band (655 nm). For shorter time delays the spectrum presents similar features to the steady state emission spectrum but, for increasing time delays, it shows a blue shift and a narrowing of the band width. If energy transfer or cross relaxation between $Cr^{3+}$ ions were present, the energy would migrate towards the lower-energy sites, giving a red shift instead of the blue shift observed. Figure 6 shows for comparison the steady state emission spectrum, obtained by excitation at 633 nm, and the spectrum for a time delay of 150 $\mu$s. It is worthwhile noting that a blue shift and a decrease in the band width of the time-resolved emission band occur. The scaled difference between both spectra is nearly Gaussian and red shifted corresponding to the luminescence losses from a small distribution of low-field sites.

## 4. Discussion

### *4.1. Fluorescence thermal quenching*

The temperature dependence of the integrated emission intensity (see section 3.1) can be related either to energy transfer or to multiphonon processes. Although energy transfer is quite common in glassy materials because of the spectral overlap between absorption and emission bands, in our case this overlap shows no appreciable temperature dependence. Moreover the blue shift of the time-resolved emission spectra when the time increases indicates that energy transfer or cross relaxation is not relevant in this case. Therefore the thermal quenching of the emission is most probably attributed to the dominance of multiphonon emission processes.

Under this assumption the experimental transition rate can be written as

$$\tau_{exp}^{-1} = \tau_R^{-1} + W_{NR} \tag{2}$$

where $\tau_{exp}$ is the measured lifetime and $\tau_R$ represents the radiative lifetime. From the measured values of the oscillator strengths at different temperatures (4.2–300 K) we find a small decrease in the radiative lifetime with increasing temperature, which is probably due to an enhancement of vibronic processes. The temperature dependence of $W_{NR}$ has been calculated from (2) using the experimental lifetimes obtained by excitation at 655 nm. As can be seen in figure 7(*a*), $W_{NR}$ rapidly increases as the temperature increases above 77 K at nearly the same rate as the luminescence decays in the same temperature interval. This enhancement of non-radiative processes is related to the low QE of $Cr^{3+}$ in glasses. At room temperature (RT) for oxide glasses the QE never exceeds 25% [4], being lower in fluoride glasses [8–11].

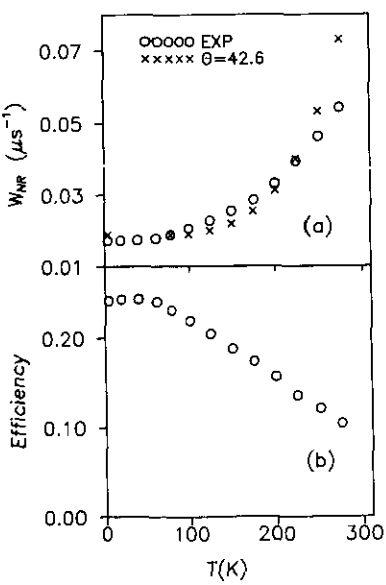


**Figure 7.** (*a*) Temperature dependence of the measured $W_{NR}$ (O) and the predicted quenching (x) assuming a different force constant in the ground and excited states for a Mannenback angle $\Theta = 42.6°$. (*b*) QE as a function of temperature.

Recently, the peculiarities of the $Cr^{3+}$ ion in different hosts have been pointed out by many workers [4, 8–11, 22]. If we bear in mind that glass is a loose structure

and take into account that, in the ground state $^4A_2$, $Cr^{3+}$ has a strong preference for sixfold octahedral coordination, it looks rather possible for the $Cr^{3+}$ ion to create a suitable arrangement of neighbouring ions when entering a glass structure. When $Cr^{3+}$ is raised from the $^4A_2$ ground state to the $^4T_2$ excited state, its coupling to the neighbouring ions is changed and the local complex of ions can adjust to a different configuration of lower energy much more easily than in a crystalline structure. In the relaxed excited state, $Cr^{3+}$ does not have the same requirements for a sixfold coordination, and therefore large configurational changes can occur, leading to larger Stokes shifts and increasing non-radiative losses.

Our previous spectroscopic studies on fluoride glasses [8–11] provided evidence that a large configurational relaxation occurs when the ion is raised to the $^4T_2$ state. Accordingly, the thermal quenching of $Cr^{3+}$ emission in fluoride glasses was discussed in terms of the QMSCC model [17] with different constant forces in the ground and excited states, and quite good agreement with the experimental results was found. We have compared the temperature dependence of non-radiative decay rates in this fluorophosphate glass with that observed in fluoride glasses and, although in this case $W_{NR}$ has the lowest values at low temperatures, it shows a similar temperature behaviour.

According to these results, we tried to fit the observed temperature dependence using the current SCC model with different force constants for the ground and excited states. Using the same procedure as in [9], we found that the best fit for the temperature dependence of $W_{NR}$ corresponds to a Manneback angle of 42.6°. Figure 7(*a*) shows the measured $W_{NR}$ and the value predicted by the QMSCC model. Calculation details can be found in [9, 17]. We made no effort to calculate absolute values of $W_{NR}$ as current theories do not seem to be adequate for this task.

The relative QEs calculated by the expression $\eta = \tau_{exp}/\tau_R$ as a function of temperature are displayed in figure 7(*b*). As can be seen, the QE rapidly falls as the temperature increases above 100 K, which is behaviour typical of $Cr^{3+}$ in glasses [2]. These low QE values are in accordance with the loose structure of glassy systems. The large rearrangement of the ionic environment between $^4A_2$ and $^4T_2$ is consistent with the observed Stokes shift, which can be related to an increase in the multiphonon emission rates [22].

### *4.2. Site-dependent effects*

*4.2.1. Fluorescence.* As we mentioned before, $Cr^{3+}$ ions occupy sites of nearly octahedral symmetry in glasses. The spread of $Dq/B$-values from site to site give a broad range of available energy levels, allowing the study of narrowing effects on the broad $^4T_2 \rightarrow {}^4A_2$ emission band as a function of laser excitation wavelength. The LNT steady state fluorescence spectra obtained by following excitations into the $^4T_1$ and $^4T_2$ absorption bands differ in the peak positions and half-widths. A narrowing (about 30 $cm^{-1}$) and a red shift (about 379 $cm^{-1}$) of the spectra can be observed as the excitation is changed from 633 to 514 nm. These results can be qualitatively understood by taking into account the spread of $Dq/B$-values from different $Cr^{3+}$ sites. When pumping with a 514 nm line on the long-wavelength edge of the $^4T_1$ band, we selectively excite a lower number of sites with smaller $Dq$-values. After a rapid non-radiative de-excitation to the lower $^4T_2$ level, these sites will give the observed narrowed fluorescence. If pumping is performed with the 633 nm line on the high-energy wing of the $^4T_2$ band, a larger number of sites can be raised to the

$^4T_2$ state, giving, after relaxation to the lower $^4T_2$ levels, the broader emission spectra observed.

These site effects are also revealed in the time-resolved excitation spectra (figure 5). Varying the emission wavelength from 780 nm to 1030 nm (high and low-energy sides, respectively, of the emission band), the spectrum shifts to longer wavelengths, corresponding to the emission from sites with smaller values of $Dq$. If we compare these results with those found in HMFGS [8], we can observe an enhancement of the narrowing and shift of the excitation spectrum monitored on the high-energy side of the emission band (see for comparison figure 7 in [8]). The excitation spectra are more sensitive to changes in the emission wavelength than to changes in the time delay. This is probably due to the similar values of the long-lived and short-lived components of the decays. Figure 5(*b*) showed the evolution of the time-resolved excitation spectra. For a long time delay (150 $\mu$s) the excitation band width decreases as a consequence of the emission losses from the low-field sites characterized by shorter relaxation times.

*4.2.2. Lifetimes.* The existence of this broad site distribution is reflected by the wavelength dependence shown by lifetimes measured along the $^4T_2 \rightarrow {}^4A_2$ emission band. Figure 3 showed the spectral dependence of average lifetimes after excitation with 510 and 655 nm laser lines. As can be seen under excitation at 655 nm (peak position of the $^4A_2 \rightarrow {}^4T_2$ absorption band), the wavelength dependence of the average lifetimes is characterized by a two-step behaviour, whereas under excitation at 510 nm (low-energy wing of the $^4A_2 \rightarrow {}^4T_1$ absorption band), a monotonic decrease in lifetimes can be observed, as would be expected if only one kind of site distribution were present. These results are therefore consistent with a model of two or more subsets of $Cr^{3+}$ ions with slightly different spectral dependences. Moreover the nearly-double-exponential character shown by the shape of lifetime curves under laser excitation reinforces this hypothesis. It is worthwhile noting the similar behaviours found by the present authors and a co-worker [8] for some HMFGS and TMFGS which could be interpreted in terms of the structural order in the host matrix. In the present case the mixed nature of the fluorophosphate seems to enhance the site-dependent effects (see for comparison the spectral dependence of average lifetimes in ZBL-type glasses in [8]). Nevertheless it is by no means clear whether $Cr^{3+}$ ions prefer to be in fluoride-like or oxygen-like surroundings.

*4.2.3. Absorption.* The observed positions of the $^2E$ and $^2T_2$ levels inside the broad $^4T_2$ absorption band are closer to some oxide than to fluoride glasses [2]. In spite of this, the value of the $\rho^2$ antiresonance parameter given in table 3 and obtained from the LNT absorption spectrum is smaller than those obtained by the present authors [21] for fluoride glasses, showing that fluorophosphate glass is a more ordered system [23].

## 5. Conclusions

(i) The optical properties of $Cr^{3+}$-doped fluorophosphate glass have been studied. From the steady state absorption and emission spectra we conclude that $Cr^{3+}$ is incorporated, on the average, in octahedrally coordinated sites. The spectroscopic data in table 1 show that $Cr^{3+}$ ions in this glass have a weak crystal field and,

therefore, the emission is characterized by a broad and structureless $^4T_2 \rightarrow {}^4A_2$ band.

(ii) The analysis of the Fano antiresonances in the long-wavelength absorption band shows that the position of levels $^2E$ and $^2T_1$ are closer to some oxide than to the fluoride glasses, although the host contains a large amount of fluoride ions. In spite of this, the value of the $\rho^2$ antiresonance parameter is smaller than those obtained by the present authors for fluoride glasses, showing that fluorophosphate glass is a more ordered system.

(iii) The QE at RT is low (about 10%) in accordance with the strong thermal quenching of the luminescence. The QMSCC model with different constant forces gives good qualitative agreement with the experimental temperature dependence of $W_{NR}$.

(iv) The narrowing observed in the steady state emission spectra when the exciting wavelength changes from 633 to 514 nm, and the spectral and time dependences of the excitation spectra, reveal the existence of a broad distribution of $Dq/B$-values in this glass. Moreover, the wavelength dependence shown by lifetimes along the $^4T_2 \rightarrow {}^4A_2$ emission band and the nearly-double-exponential behaviour of the decays provide evidence for the existence of two statistical site distributions for $Cr^{3+}$.

(v) The mixed nature of the fluorophosphate glass seems to enhance the site-dependent effects in comparison with fluoride glasses. Nevertheless it is by no means clear whether $Cr^{3+}$ ions prefer to be in fluoride-like or oxygen-like surroundings.

## Acknowledgments

The authors would like to thank A de Pablo from the Instituto de Cerámica y Vidrio (Arganda del Rey) for the fluorophosphate sample preparation. This work was supported by the Comisión Interministerial de Ciencia y Tecnología of the Spanish Government (No 0188/89), and the Basque Country Government (No PGV 9012).

## References

[1] Bates T 1962 *Modern Aspects of the Vitreous State* Vol 2, ed J D Macken (London: Butterworth) ch 5
[2] Andrews L J, Lempicki A and McCollum B C 1981 *J. Chem. Phys.* **74** 5526
[3] Bergin F J, Donegan J F, Glynn T J and Imbusch G F 1987 *J. Lumin.* **36** 231
[4] Imbusch G F, Glynn T J and Morgan G P 1990 *J. Lumin.* **45** 63
[5] Rasheed F, O'Donnell K P, Henserson B and Hollis D B 1991 *J. Phys.: Condens. Matter* **3** 1915
[6] Rasheed F, O'Donnell K P, Henserson B and Hollis D B 1991 *J. Phys.: Condens. Matter* **3** 3825
[7] Yamaga M, Henderson B, O'Donnell K P and Gao Y 1991 *Phys. Rev.* B **44** 4853
[8] Balda R, Fernández J, Illarramendi M A, Arriandiaga M A, Lucas J and Adam J L 1991 *Phys. Rev.* B **44** 4759
[9] Illarramendi M A, Fernández J, Balda R, Lucas J and Adam J L 1991 *J. Lumin.* **47** 207
[10] Fernández J, Illarramendi M A, Balda R, Arriandiaga M A, Lucas J and Adam J L 1991 *J. Non-Cryst. Solids* **131–133** 1230
[11] Balda R, Fernández J, Elejalde M J, Illarramendi M A and Jacoboni C 1991 *J. Phys.: Condens. Matter* **3** 7695
[12] Henderson B, Yamaga B, Gao Y and O'Donnell K P 1992 *Phys. Rev.* B **46** 652
[13] Sugano S, Tanabe Y and Kamimura H 1970 *Multiplets of Transition-Metal Ions in Crystals* New York: Academic)

[14] Kenyon P T, Andrews L J, McCollum B C and Lempicki A 1982 *IEEE J. of Quantum Electron.* **QE-18** 1189
[15] Reisfeld R 1985 *Mater. Sci. Eng.* **71** 375
[16] Yen W M 1986 *Optical Spectroscopy of Glasses* ed I Zschokke (Dordrecht: Reidel)
[17] Struck C W and Fonger W H 1975 *J. Lumin.* **10** 1
[18] Tischer R E 1968 *J. Chem. Phys.* **48** 4291
[19] Fano U 1961 *Phys. Rev.* **124** 1866
[20] Fano U and Cooper J W 1965 *Phys. Rev.* **137** A1364
[21] Illarramendi M A, Fernández J and Balda R 1992 *J. Lumin.* **53** 461
[22] Payne S A, Chase L L and Krupke W F 1987 *J. Chem. Phys.* **86** 3455
[23] Lempicki A, Andrews L, Nettel S J, McCollum B C and Solomon E I 1980 *Phys. Rev. Lett.* **44** 1234